www.amlett.com, www.vbripress.com/aml, DOI: 10.5185/amlett.2015.5869 Published online by the VBRI Press in 2015

Dual mode emission in $NaYF_4$:Yb Er nanorods for photovoltaics application

Ashwani Kumar[1,2], Surya Kant Tripathi[3], Abhay D. Deshmukh[4*]

[1]*Department of Physics, Chandigarh University, Gharuan, Mohali, India*
[2]*Department of research, innovation & consultancy, Punjab Technical University, Jalandhar, India*
[3]*Department of Physics, Punjab University Chandigarh, Chandigarh, India*
[4]*Energy Materials and Devices Laboratory, Department of Physics, RTM Nagpur University, Nagpur, India*

[*]Corresponding author. Tel: (+91) 7122041093; E-mail: abhay.d07@gmail.com

Received: 24 February 2015, Revised: 25 March 2015 and Accepted: 27 March 2015

ABSTRACT

In the present study, synthesis, characterization, of dual mode emission (Up and downconversion) in lanthanide-doped $NaYF_4$ nanorods is presented. The unique and rich energy-level structure of these lanthanide ions allows for efficient spectral conversion, including up and downconversion processes mediated by resonant energy transfer between neighboring lanthanide ions. The careful examination of nanorods indicates the perfect uniformity, monodispersity and well defined crystallographic facets. Er^{3+}, Yb^{3+} doped NCs exhibit green/red dual mode emission with low power density. As solar cells have majority of losses due to spectral mismatch, so with the help of these dual mode emission of nanorods can be utilized as up/down converter to increase the efficiency solar cell. Copyright © 2015 VBRI Press.

Keywords: Dual mode emission; nanorods; upconversion; downconversion.

Introduction

Adapting the solar spectrum, has received attention nowadays, the spectrum can be changed by two methods, upconversion and downconversion, which are capable of reducing energy losses due to spectral mismatch. In the case of upconversion, two low-energy (infrared) photons are 'added up' to give one higher-energy photon [**1**] thus converting sub-bandgap photons, which are otherwise lost, into supra-bandgap photons, which can be absorbed [**2, 4**]. The numerous studies on the synthesis and spectroscopic properties of upconverting nanocrystals [**5-14**] (NCs) for improving the efficiency of solar cell has been reported [**15-17**]. The opposite process, down-conversion, is defined as the 'cutting' of one high-energy photon into two lower-energy photons. This process can reduce the energy loss related to the thermalization of hot charge carriers after the absorption of a high-energy photon. By cutting one high-energy photon into two low-energy photons, which can both be absorbed by the solar cell, current doubling is obtained in the upper region of the solar spectrum, which consists of photons with energies exceeding 2E [**18**].

In the present study, we explored the possibilities of efficient up- and downconversion of a single visible or ultraviolet photon into two near-infrared (NIR) photons using lanthanide ions. The unique and rich energy-level structure of these ions allows for efficient spectral conversion, including up and downconversion processes mediated by resonant energy transfer between neighbouring lanthanide ions. $NaYF_4$ was chosen as the host lattice to study the up- and downconversion scheme leads to efficient energy transfer. The choice was motivated by it low phonon energy (maximum phonon energy is 400 cm^{-1}) it will be quite interesting and informative to study different luminescence processes with single and double dopants. The Raman spectrum of undoped [**19**] $NaYF_4$ has been shown to have three fully resolved phonon peaks at 298, 370 and 418 cm^{-1} with a weighted average of close to 360 cm^{-1}. This is considerably lower than other similar structured fluoride host lattices [**20**] such as $LiYF_4$ which has phonon energies up to 570 cm^{-1}. In order to have the efficient DC it is crucial to have a nonradiative decay from the $^4F_{7/2}$ level to the $^4S_{3/2}$ level since DC from the $^4S_{3/2}$ level is difficult. Spectral conversion for solar cells using this DC scheme is promising as the efficiency gain higher due the large section of the solar spectrum available in the wavelength region in the 490 nm and emission from this couple falls in the category of crystalline Si cell absorption.

Experimental

Materials

RE doped $NaYF_4$ NCs were synthesized via precipitation method. All the chemicals used were of analytical reagent grade and were used as obtained from the manufacturer with further purification. The glass beakers were cleaned in ethanol and acetone, and finally ultrasonically cleaned for 30 minutes in distilled water.

Briefly, the lanthanides (Y^{3+}, Er^{3+} and Yb^{3+}) chlorides were prepared by reacting Y_2O_3, Yb_2O_3 and Er_2O_3 with

HCl. NaCl chosen as the source of Na ions. The $NaYF_4$: Yb,Er phosphor was obtained by precipitation with drop wise addition of HF into the chloride solution. The resulting precipitates were stirred for the one hour and were separated via centrifugation at 10000 rpm; further washed three times with de-ionized water. The resulting mixture was dried in oven at 80ºC for 12 hrs. After drying, the prepared phosphor was heated for 2 hr at 700ºC. X–ray diffraction (XRD) of the powder samples were examined on a Brukers D8 Focus diffractometer using Cu Kα radiation (λ=0.15405 nm). Scanning electron microscopy (SEM) micrographs were recorded with ZEISS EVO MA-10. The upconversion emission spectra were obtained using a LIMO fiber-coupled F6 series 978 nm laser diode (maximum power of 30W (CW), at 40 A LDC, as excitation source. A 200 µm optical fiber was used. Light beam from the fiber was collimated and focused by a set of plano-concave lenses. The samples were studied with laser output power of 100 mW. For the upconversion studies, the nanocrystal samples were placed in quartz holder. The upconverted visible emission was collected at right angle with respect to the incident beam and spectra was obtained using portable spectrometer of AVANTES-AvaSpec-USB2 with AVASOFT 7.3 software. The detailed experimental setup is shown in the supporting information (**Fig. 1**). Emission spectra for DC and life time studies were made on system F900 of Edinburgh instruments.

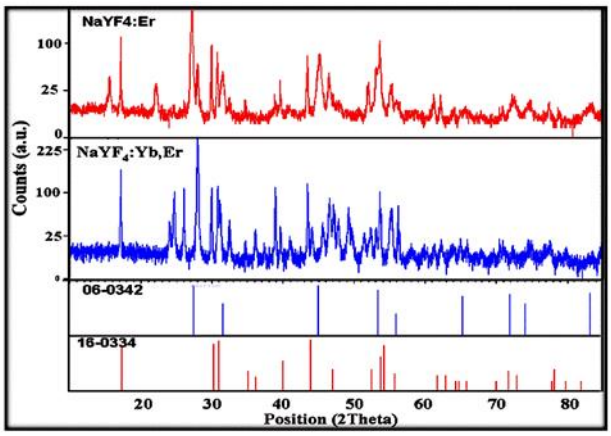

Fig. 1. XRD pattern of $NaYF_4$: Er (2%) and $NaYF_4$: Er (2%),Yb (18%)

Results and discussion

Fig. 1 shows the X-ray powder diffraction (XRD) pattern of the prepared product obtained with $NaYF_4$: Er (2%) and $NaYF_4$: Er (2%),Yb (18%). The XRD pattern of the material confirms its hexagonal crystalline phase and most of the strong peaks match with those of standard β-$NaYF_4$ (PDF card No. 00-016-0334/ 00-028-1192) and α- $NaYF_4$ (PDF card No. 006-0342).

The SEM images provide direct information about the size, growth and typical shape of the as-synthesized $NaYF_4$ sample. **Fig. 2** illustrates the representative SEM images of $NaYF_4$ prepared using HF as fluoride source. The product obtained composed of a great deal of nanorods with uniform size of nearly 200 nm in length and 100 nm in diameter.

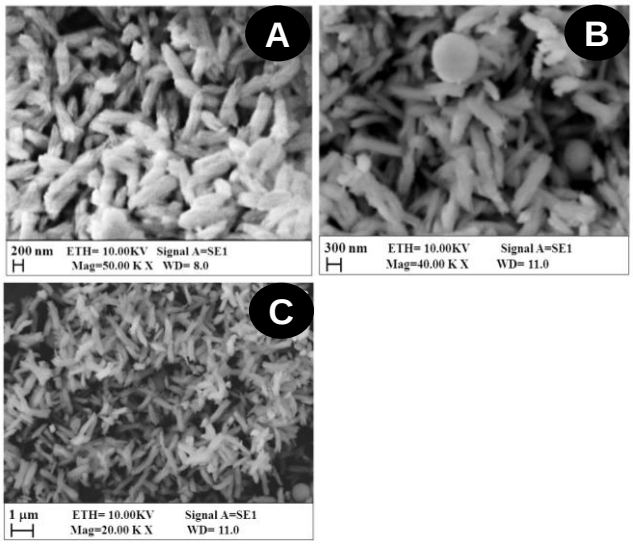

Fig. 2. Morphology of $NaYF_4$:Er(fig. a and fig b),(c) $NaYF_4$:Yb,Er.

The magnified SEM image shows clearly that the nanorods are of rough surfaces as well as sharp and crack ends. More careful examination of a typical rod indicates the perfect uniformity, monodispersity and well defined crystallographic facets. It is worthy to note that the top end of the rod is like hexagonal prism like a crown not flat one. The growth process is much like the growth process of the snowflake, which also adopts with the hexagonal crystal structure. The difference is that the snowflake developed on the plane to form six petals morphology, while the β-$NaYF_4$ hexagonal prism developed along the c axis to form a crown-like top end. Similar characteristic also can be observed on the β-$NaYF_4$ hexagonal flakes. Besides the hexagonal phase, cubic phase with spherical morphology is also observed (**Fig. 2b**). The Yb^{3+} doping in the phosphor shows the sharp edges in SEM micrographs (**Fig. 2c**). The incorporation of Yb into the lattice of NaYF4 improves the crystallinity and better nanorod formation. Added impurities may influence the size and morphology of a given crystal by participating in the nucleation and growth, in which many overall factors integrate to dominate the process. However, Yb^{3+} introduction helps hexagonal phase formation revels in diffraction pattern.

The emission spectra of $NaYF_4$: Er (2%) and $NaYF_4$: Er (2%), Yb (20%) is shown in **Fig. 3**. In sample doped with Er^{3+} only, excitation with 364/378 nm raises exaction to $^4G_{9/2}$ and $^4G_{11/2}$ level and yields emission from $^4S_{3/2}$, $^4F_{9/2}$ and $^2H_{11/2}$ levels, but not from the $^4F_{7/2}$ level. The emission spectra show the same Er^{3+} emission for both excitation, but with different relative intensities. It is found that the Yb^{3+} introduction has no influence on the intensity ratio of $^4S_{3/2}$ and $^4F_{9/2}$ emission. Population of the $^4S_{3/2}$ and $^4F_{9/2}$ of Er^{3+}states is performed by multistep phonon relaxation from both $^4G_{9/2}$ and $^4G_{11/2}$ levels. With the introduction of Yb^{3+} ions, the $^4S_{3/2}$ emission intensity decreases while intensity of emission from $^4F_{9/2} \rightarrow {}^4I_{15/2}$ transition increases. The increase in $^4F_{9/2}$ emission is explained by efficient cross relaxation between Er^{3+} and Yb^{3+} i.e. Er^{3+} ($^4G_{11/2} \rightarrow {}^4F_{9/2}$) and Yb^{3+} ($^2F_{7/2} \rightarrow {}^2F_{5/2}$). The increase in $^4F_{9/2}$ emission with the introduction of Yb^{3+} ions indicates that a cross relaxation energy transfer enhances the $^4F_{9/2}$ state

population and decrease the population on $^4S_{3/2}$ state. The energy mismatch for the $^4G_{11/2}$ relaxation process is small about 800 cm^{-1} and can be accommodated by a two phonon emission process. This process populates the $^4F_{9/2}$ level which gives the characteristic red emission of Er^{3+}. At the same time, Yb^{3+} is raised to the $^2F_{5/2}$ excited state. However the energy gap for $^4G_{9/2}$ level is 1800 cm^{-1} and requires bridging by five phonons. Therefore multiphonon relaxation will be slow and cross relaxation can compete with non-radiative multistep relaxation. Considering the energy matching condition, the possible resonant process are $^4G_{11/2}$ (Er^{3+}) + $^2F_{7/2}$ (Yb^{3+}) → $^4F_{9/2}$ (Er^{3+}) + $^2F_{5/2}$ (Yb^{3+}) and $^2H_{11/2}$ (Er^{3+})+ $^2F_{7/2}$ (Yb^{3+}) → $^4I_{11/2}$ (Er^{3+}) + $^2F_{5/2}$ (Yb^{3+}).

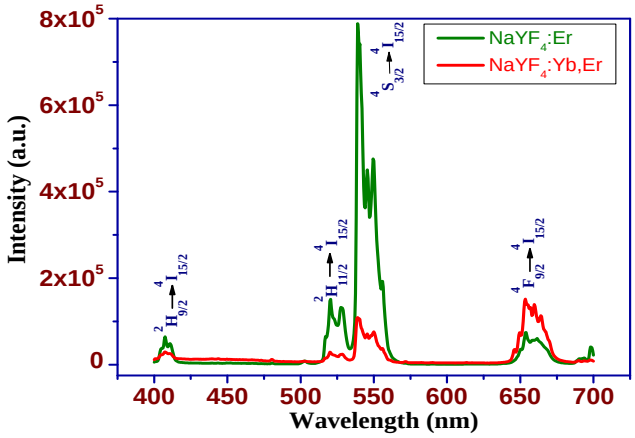

Fig. 3. Emission spectra of $NaYF_4$:Er, NaYF4:Yb,Er (Ex=378nm).

The excitation spectrum for $^4S_{3/2}$ level (Suppl. **Fig. 2**) composed of the main excitation line which can be assigned from the $^4I_{15/2}$ ground level to different excited states of Er^{3+} i.e. $^2G_{7/2}$ (254 nm), $^4G_{9/2}$ (364 nm), $^4G_{11/2}$ (378 nm), $^2H_{9/2}$ (410 nm), $^4F_{5/2}$ (450 nm) and $^4F_{7/2}$ (488 nm). Based on the luminescence properties, the photon conversion mechanism under above mentioned excitations have been proposed, as shown in **Fig. 4**, Energy Level Diagram. The emission spectra for 448 nm and 488 nm are shown in **Fig. 5**. Under the 448 nm excitation, the Yb^{3+} introduction has no influence on the intensity ratio of red emission to the green one. It has shown the emission from the $^4S_{3/2}$ and $^2F_{9/2}$ levels, but no emissions from the $^4F_{7/2}$ level is observed. This shows that nonradiative relaxation form this level to the next lower level $^2H_{11/2}$ is fast and radiative decay from the $^4F_{7/2}$ level cannot compete with nonradiative process (typically around 1300 cm^{-1}).

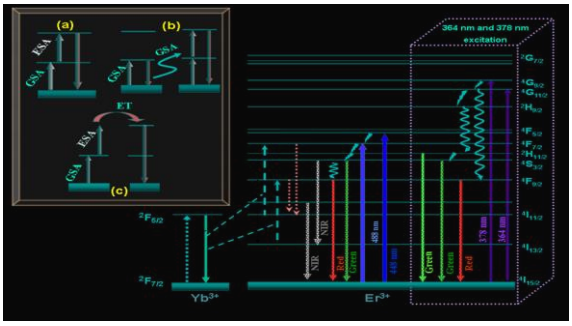

Fig. 4. Energy level scheme of the Er^{3+} and Yb^{3+} couple showing possible mechanisms for the different excitations for DC.

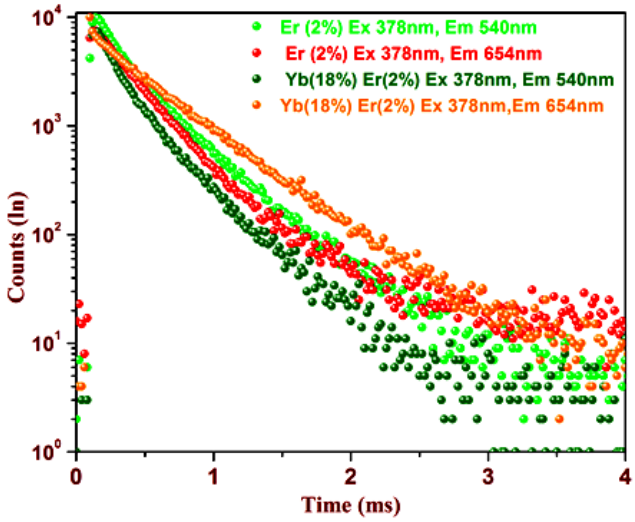

Fig. 5. Luminescence decay curves for the $^4S_{3/2}$ and $^4F_{9/2}$ emission in $NaYF_4$:Er and $NaYF_4$:Yb,Er measured at room temperature. The excitation wavelength is 378 nm and Emission is 540 nm and 654 nm.

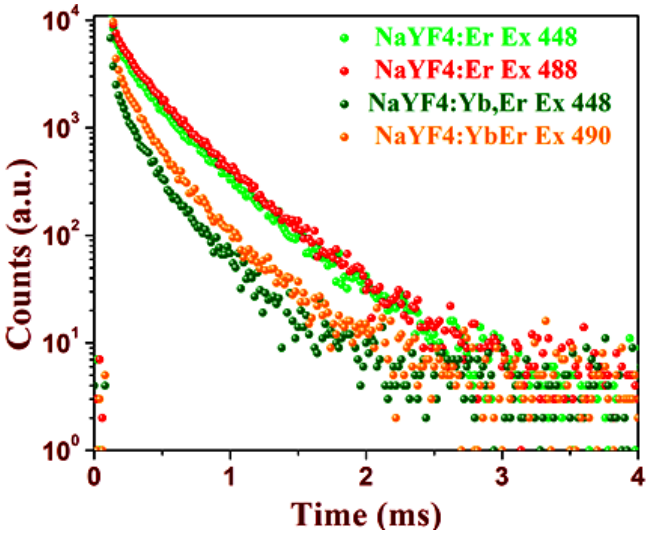

Fig. 6. Luminescence decay curves for the $^4S_{3/2}$ emission in $NaYF_4$: Er and $NaYF_4$:Yb, Er measured at room temperature. The excitation wavelength is 448 nm and 488/490 nm and Emission is 540 nm.

After fast multiphonon relaxation to the $^2H_{11/2}$ level, further relaxation to the $^4S_{3/2}$ level occurs. Emission from $^4S_{3/2}$ level is observed to be increased by Yb^{3+} doping while the emission from $^4F_{9/2}$ is quenched. The spectral band shapes and positions are similar to some extent those obtained upon 488nm excitation, as reported by others,[21] except the emission at 850 nm. The mechanism for this emission can be attributed to either an energy transfer (ET) process or excited state observation (ESA). The origin of NIR luminescence of this Er^{3+} doped phosphor is suggested as follows: the 488 nm excites the Er^{3+} ions into the $^4F_{5/2}$ states, which can nonradiatively decay to the $^4S_{3/2}$ via $^4F_{7/2}$ and $^4H_{11/2}$ intermediate levels. From the $^4S_{3/2}$ level, it rediatively decays to the $^4I_{15/2}$ and $^4I_{13/2}$ level results in the green and NIR emission. However, non-radiative decay from the $^4F_{7/2}$→ $^4I_{11/2}$ and $^4S_{3/2}$→ $^4I_{13/2}$ excites the Yb^{3+} ions to $^2F_{5/2}$ level and this energy again transfer to the Er^{3+} ions. Simultaneously Er^{3+} to Er^{3+} energy transfer can be possible(inset of Figure 4); since the energy difference

between $^4I_{11/2}$ and $^4F_{9/2}$ level is identical to the difference between $^4I_{9/2}$ and $^4I_{13/2}$ levels, the two Er ions undergo ion pair process ($^4I_{9/2}$, $^4I_{11/2}$) → ($^4I_{13/2}$, $^4F_{9/2}$). The back energy transfer from Yb^{3+} ions to Er^{3+} excites the Er^{3+} ions to $^4F_{7/2}$ level from the $^4I_{11/2}$ level, hence increased in the NIR emission observed. Further work is necessary to identify the main mechanism for the observed NIR emission from $^4S_{3/2}$ → $^4I_{11/2}$.

The lifetime of excited states can be used to reveal the surroundings of luminescent centers of Er^{3+} and Yb^{3+}. When excited wavelength was 378 nm, only Er^{3+} ions could be excited and thus the information for luminescence environment of the Er^{3+} could be obtained from the decay curves of emission $^4S_{3/2}$ and $^4F_{9/2}$ under $^4G_{11/2}$ excitation.

Fig. 5 shows the $^4S_{3/2}$ and $^4F_{9/2}$ luminescence decay curves (excited by $^4G_{11/2}$) of Yb^{3+} doped and undoped $NaYF_4$:Er^{3+}. The sample without Yb^{3+}, presented a longer $^4S_{3/2}$ lifetime compared to Yb^{3+} doped $NaYF_4$:Er^{3+} one, which indicate that $^4S_{3/2}$ level populates less with incorporation of Yb^{3+} ions. However the $^4F_{9/2}$ level lifetime is lesser (307µs) for undoped phosphor. For the sample without Yb^{3+}, the $^4S_{3/2}$ emission decay is exponential with a decay time of 577µs. As the Yb^{3+} ions are incorporated into the system, the decay of $^4S_{3/2}$ emission becomes faster and nonexponential. This is due to the energy transfer to neighboring Yb^{3+} ions. This decrease in the decay of $^4S_{3/2}$ level is explained by the fact that each Er^{3+} donor has a different distribution of Yb^{3+} acceptors around it. As mentioned above the sample without Yb^{3+} shows the decreased decay time for $^4F_{9/2}$ emission with nearly single exponential decay of 276µs, while for the sample with Yb^{3+} has nonexponential decay of 507µs. This is because of the efficient population of $^4F_{9/2}$ level by cross relaxation with neighboring Yb^{3+} ions [Er^{3+} ($^4G_{11/2}$→ $^4F_{9/2}$) and Yb^{3+} ($^2F_{5/2}$→ $^2F_{7/2}$)]. The decay time of $^4F_{9/2}$ emission depends on the Yb^{3+} ions shows that energy transfer from $^4F_{9/2}$ level for Er^{3+} to Yb^{3+} is efficient.

Decay curves for the $^4F_{5/2}$ and $^4F_{7/2}$ excitation were also recorded for both the samples (shown in **Fig. 6**), demonstrating that there was energy transfer from $^4F_{9/2}$ level of Er^{3+} to the $^2F_{5/2}$ level of Yb^{3+} also at room temperature. This is consistent with the observation that the $^4S_{3/2}$ and $^4F_{9/2}$ emission was weak while the $^4I_{9/2}$ emission is stronger. Upon excitation with 448nm, the sample without Yb^{3+} showing the decay time of 273µs and 327µs for sample with Yb^{3+} for $^4S_{3/2}$ emission. Moreover excitation with $^4F_{7/2}$, the single exponential decay was observed (357µs) for the $^4S_{3/2}$ emission. Since the emission form $^4F_{9/2}$ level is very weak for $^4F_{5/2}$ and $^4F_{7/2}$ excitation for both samples, a stronger emission in the NIR region resulted.

Fig. 7 shows the corresponding upconversion emission spectra of $NaYF_4$:2% Er^{3+} and $NaYF_4$:18% Yb^{3+}, 2% Er^{3+} upon irradiation with a diode laser at 980 nm of 100 mW. In all cases, upconverted emission was observed in the blue, green, red, and NIR spectral regions. Blue emission (very weak at this power) was observed at ~415 nm from the $^2H_{9/2}$ →$^4I_{15/2}$, transition while green emissions were observed at ~510–560 nm ascribed to transitions from the $^2H_{11/2}$ and $^4S_{3/2}$ excited states to the $^4I_{15/2}$ ground state (centered at 522 and 554 nm, respectively). Furthermore, red emission was observed between 630–680 nm from the $^4F_{9/2}$ and $^2F_{9/2}$ excited state to the ground state and peaked at 654 nm and 660 nm respectively. A comparatively weaker NIR emission between 760–870 nm, ascribed to the $^4I_{9/2}$→$^4I_{15/2}$ transition with peak at 800 nm, and the $^4S_{3/2}$→$^4I_{13/2}$ transition at 845 nm. The optical photograph shows the green color for $NaYF_4$:2% Er^{3+} and yellowish green color for $NaYF_4$:18% Yb^{3+}, 2% Er^{3+} phosphors (inset of **Fig. 7**).

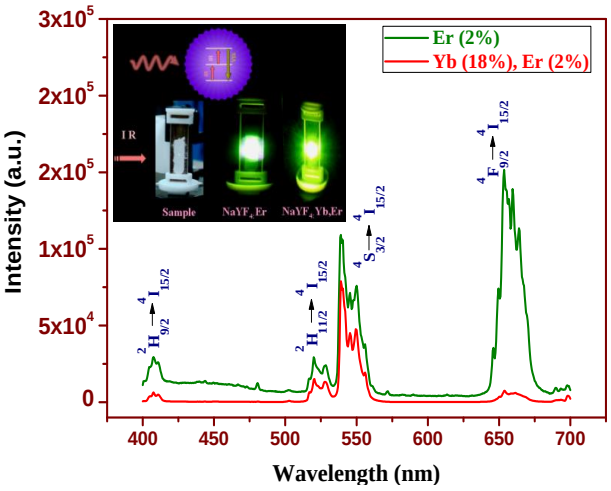

Fig. 7. Upconversion emission spectra of $NaYF_4$:Er, $NaYF_4$:Yb, Er.

The green emitting states ($^2H_{11/2}$, $^4S_{3/2}$) are populated via a two-photon process, typical of Er^{3+}/Yb^{3+} materials. The population of these states usually occurs via two successive energy transfers from Yb^{3+} ions (both in the $^2F_{5/2}$ excited state) to the Er^{3+} ion, exciting it first to the $^4I_{11/2}$ intermediate state and subsequently to the $^4F_{7/2}$ excited state [Suppl. **Fig. 3**]. The ion decays non-radiatively to the lower-lying $^2H_{11/2}$ and $^4S_{3/2}$ levels and follows radiative path to ground state resulting in the observed green emission. Alternatively, it can decay non-radiatively to the $^4F_{9/2}$ state leading to red emission. The $^4F_{9/2}$ state can also be populated via another two-photon mechanism, which directly excites the state, as opposed to population from non-radiative relaxation of the upper $^4S_{3/2}$ state. Following the initial Yb^{3+} to Er^{3+} energy transfer, the Er^{3+} ion in the $^4I_{11/2}$ excited intermediate state can decay non-radiatively to the lower-lying $^4I_{13/2}$ state. A subsequent transfer of energy from an excited Yb^{3+} ion brings the ion directly to the $^4F_{9/2}$ state. A further such transfer can excite the Er^{3+} ion from the $^4F_{9/2}$ state to the $^2H_{9/2}$ state and leads to the observed red $^2H_{9/2}$→$^4I_{11/2}$ emission. The upconversion spectra presented in figure 4 reveals distinct difference between the $NaYF_4$:2% Er^{3+} and $NaYF_4$:18% Yb^{3+}, 2% Er^{3+}. Most obvious difference lies in the intensity of the upconversion emission as well as green to red ratio.

To account for the appearance of the relatively strong red emission, the population mechanism of the $^4F_{9/2}$ level should be clarified. The red emission ($^4F_{9/2}$ → $^4I_{15/2}$) can be produced following two processes: one is via a nonradiative relaxation through the $^4S_{3/2}$ level; the other is direct population from the $^4I_{13/2}$ level, which can be realized through the nonradiative decay of the $^4I_{11/2}$ level. Both mechanisms underline the importance of multiphonon relaxation through which the red upconversion emission is generated. Vetrone et al[22] came to the conclusion that nanocrystalline materials possess a higher probability of

multiphonon relaxation compared with their bulk counterpart, and the nonradiative relaxation rate of $^4I_{11/2} \rightarrow ^4I_{13/2}$ is larger in the nanocrystals. It was shown that in Er^{3+}/Yb^{3+} codoped systems the $^4F_{9/2}$ level was populated via the nonresonant $^4I_{13/2} \rightarrow ^4F_{9/2}$ transition since small excess energy is easily dissipated into the host lattice. In the investigated case, the difference in the upconversion spectrum between different samples is related to the stability of the intermediate state - $^4I_{13/2}$ and it will favor red upconversion emission.

Conclusion

In conclusion, we have demonstrated potential photon conversion processes (dual mode emision) in $NaYF_4$:Er and $NaYF_4$:Yb, Er. This dual mode emission of lanthanide doped $NaYF_4$ nanorods can enhance the efficiency of a solar cell, if photons absorbed by the up/down-converter, converts to higher spectral response of solar cell. It has been calculated that ideal spectral downconversion would increase the Shockley-Queisser limit upto 40% for p-n semiconductor solar cells with bandgap of 1.05 eV, which is very close to band gap of c-Si [**18**]. The present results demonstrate the potential of spectral down/upconversion achieved by lanthanide ions for reducing energy loss in photovoltaic devices and increasing the efficiency of c-Si solar cells making them more cost-effective.

Acknowledgements
One of the author A.D.D is thankful to Nagpur Uvniersity for financila support under University Project Scheme (grant No. 1345).

Reference

1. Auzel, F. *Chem. Rev*. **2004**, *104*, 139. **DOI:** 10.1021/cr020357g
2. Shalav, A.; Richards, B. S.; Trupke, T.; Kramer, K. W.; Gudel, H. U. *Appl. Phys.Lett*. **2005**, *86*, 013505. **DOI:** 10.1038/nphoton.2012.158
3. Trupke, T.; Green, M. A.; Wurfel, *P. J. Appl. Phys*. **2002**, *92*, 4117. **DOI:** 10.1063/1.1505677
4. (a) Trupke, T.; Green, M. A.; Wurfel, *P. J. Appl. Phys.* **2002**, *92*, 1668.; (b) Richards, B. S. Sol. *Energy Mater. Sol. Cells* **2006**, *90*, 1189. **DOI:** 10.5772/39213
5. Heer, S.; Kompe, K.; Gu¨del, H. U.; Haase, *M. Adv. Mater*. **2004**, *16*, 2102. **DOI:** 10.1002/adma.200400772
6. Lu, H.; Yi, G.; Zhao, S.; Chen, D.; Guo, L.-H.; Cheng, *J. J. Mater. Chem.* **2004**, *14*, 1336. **DOI:** 10.1039/B315103D
7. Yi, G.; Lu, H.; Zhao, S.; Ge, Y.; Yang, W.; Chen, D.; Guo, *L.-H. Nano Lett.* **2004**, *4*, 2191. **DOI:** 10.1021/nl048680h
8. Sivakumar, S.; Veggel, F. C. J. M. V.; Raudsepp, *M. J. Am. Chem. Soc*. **2005**, *127*, 12464. **DOI:** 10.1021/ja052583o
9. Suyver, J. F.; Aebischer, A.; Biner, D.; Gerner, P.; Grimm, J.; Heer, S.; Kra¨mer, K. W., Reinhard, C.; Gudel, *H. U. Opt. Mater*. **2005**, *27*, 1111. **DOI:** 10.1016/j.optmat.2004.10.021
10. Wang, L.; Yan, R.; Huo, Z.; Wang, L.; Zeng, J.; Bao, J.; Wang, X.; Peng, Q.; Li, Y. Angew. *Chem., Int. Ed.* **2005**, *44*, 6054. **DOI:** 10.1002/anie.200501907
11. Zeng, J.-H.; Su, J.; Li, Z.-H.; Yan, R.-X.; Li, Y.-D. *Adv. Mater*. **2005**, *17*, 2119. **DOI:** 10.1002/adma.200402046
12. S. Som, M. Chowdhury, S. K. Sharma, *J Mater Sci*., **2014,** *49*, 858. **DOI:** 10.1007/s10853-013-7769-8
13. Anurag P., S. Som, V.K., V. K. K,. Kumar,. Rai, V. K, Swart H.C., *Sensors and Actuators B*, **2014,** *202*, 1305. **DOI:** 10.1016/j.snb.2014.06.074
Das, S Reddy A. A., Babu S. S., Prakash G V., *Materials Letters*, **2014**, *120*, 232. **DOI:** 10.1016/j.matlet.2014.01.013
14. Mac Queen R. W, Schulze T. F., Khoury T., Cheng Y. Y.,. Stannowski B,. Lips K, Crossley M. J., Schmidt T., *Proc. SPIE*, **2013**, *8824*, 882408. **DOI:** 10.1117/12.2026907
15. Naccache R., Vetrone F., Capobianco J.A., *Chem Sus Chem*, **2013**, *6*, 1308**.** **DOI:** 10.1002/cssc.201300362
16. Trupke T., Green M. A., Würfel P., *J. Appl. Phys.* **2002**, *92*, 4117. **DOI:** 10.1063/1.1505677
17. (a) Trupke, T.; Green, M. A.; Wurfel, P. J. Appl. Phys. **2002**, *92*, 1668, b) B. S. Richards, Sol. Energy Mater. Sol. Cells **2006**, *90*, 1189. **DOI:** 10.5772/39213
18. Suyver, J.; Grimm, J.; Van Veen, M.; Biner, D.; Kramer K.; Gudel, H. J. Lumin., **2006**, *117*, 1. **DOI:** 10.1007/s10853-007-2266-6
19. Miller, S.; Rast H.; Caspers, H. The J. of Chem. Phys, **1970**, 4172, 52.
20. Aarts, L.; Van der Ende, B.M.; Meijerink, A. J. App. Phys., 2009, *106*, 023522. **DOI:** 10.1063/1.3177257
21. Vetrone F,; Boyer J C,; Capobianco J A,; Speghini A; Bettinelli M. J. Appl. Phys. **2004,** *96*, 661. **DOI:** 10.1063/1.1739523

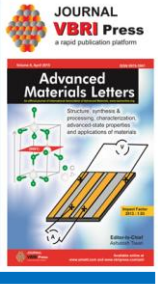

Supporting information

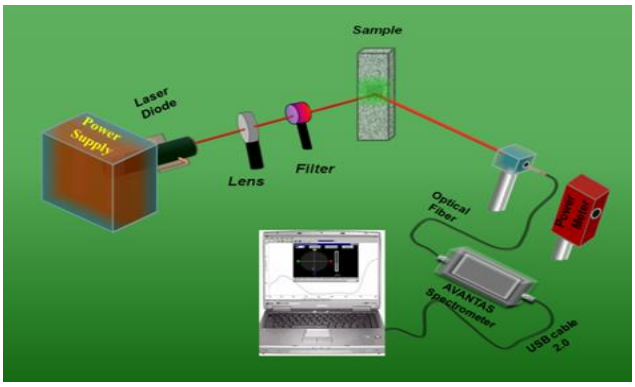

Fig. 1. Experimental setup of up-conversion luminescence.

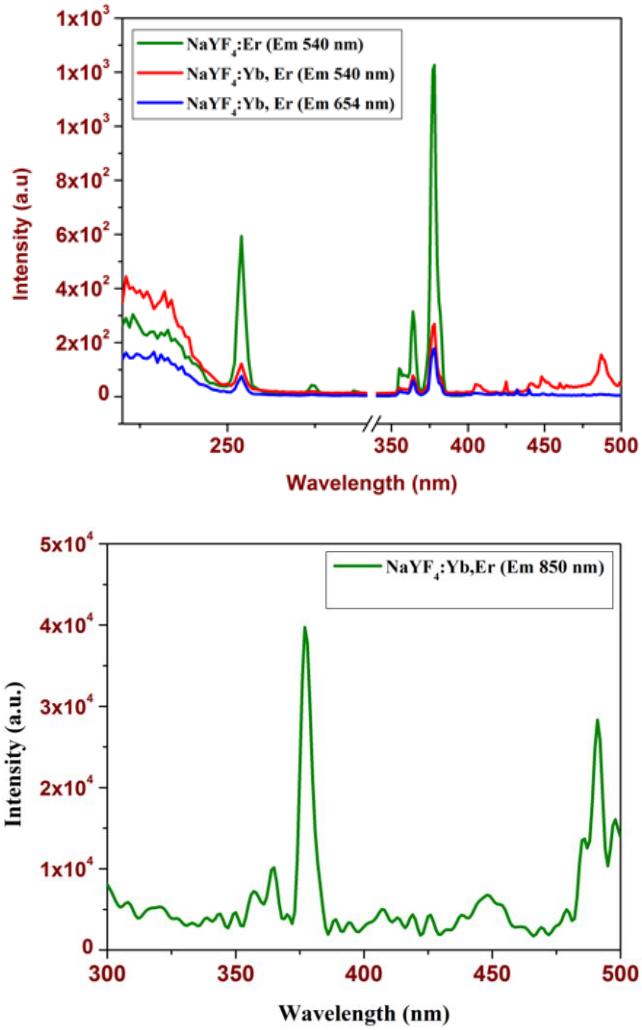

Fig. 2. Excitation spectra of $NaYF_4$:Er, Yb and $NaYF_4$:Er.

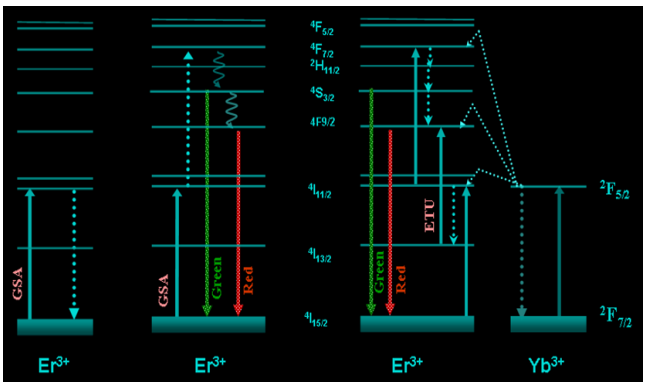

Fig. 3. Energy level mechanism in Er-Er and Yb-Er couple for upconversion luminescence by 980.